MODELLING OF KINETICS OF AUSTENITE FORMATION IN STEELS WITH DIFFERENT INITIAL MICROSTRUCTURES

F. G. CABALLERO, C. CAPDEVILA and C. GARCÍA DE ANDRÉS

Dr. F.G. Caballero and Dr. C. Capdevila, Post-doctoral Research Assistants, and Dr. C. García de Andrés, Research Scientist, are in the Department of Physical Metallurgy, Centro Nacional de Investigaciones Metalúrgicas (CENIM), CSIC, Avda. Gregorio del Amo, 8, 28040 Madrid, Spain.

Abstract

The main aim of this work is to study the mechanisms that control the austenitisation process in steels with different initial microstructures. The compiled knowledge in literature regarding the isothermal formation of austenite from different initial microstructures (pure and mixed microstructures), has been used in this work to develop a model for non-isothermal austenite formation in steels with initial microstructure consisting of ferrite and/or pearlite. The microstructural parameters that affect the nucleation and growth kinetics of austenite, and the influence of the heating rate have been considered in the modelling. Moreover, since dilatometric analysis is a technique very often employed to study phase transformations in steels, a second model to describe the dilatometric behaviour of the steel and calculate the relative change in length which occurs during the austenite formation has been developed. Both kinetics and dilatometric models have been validated. Experimental kinetic transformation, critical temperatures as well as the magnitude of the overall contraction due to austenite formation are in good agreement with calculations.

Key Words: Modelling, Continuous Heating Transformations, Kinetics.

1. Introduction

Most commercial processes rely on heat treatments which cause the steel to revert to the austenitic condition. This includes the processes involved in the manufacture of wrought steels and in the fabrication of steel components by welding. The formation of austenite is an inevitable occurrence during the heat treatment of steels. The phenomenon of austenitisation has been studied in the past but the work has tended to be disconnected and qualitative.[1-14)] The initial condition of the austenite determines the development of the final microstructure and mechanical properties, so the modelling of the transformation into austenite is useful. In this sense, a quantitative theory dealing with the nucleation and growth of austenite from a variety of initial microstructural conditions is vital.[15)]

On the other hand, little information is available about the austenite formation in steels subjected to continuous heating.[16)] Recent work has quantitatively modelled the transformation of an ambient temperature steel microstructure into austenite during continuous heating.[17,18)] An Avrami equation, which is generally used to model transformations under isothermal conditions, was applied successfully to the pearlite-to-austenite transformation during continuous heating in a eutectoid steel with a fully pearlitic initial microstructure. Lately, some researchers have adopted a different approach to the problem using artificial neural network;[19,20)] this has helped to identify the fact that a neglect of the starting microstructure can lead to major errors in the transformation temperatures, sometimes by more than 100 °C.

The formation of austenite during heating differs in many ways from those transformations that occur during the cooling of austenite. For instance, the kinetics of austenite decomposition can be described completely in terms of the chemical composition and the austenite grain size. By contrast, the microstructure from which austenite may form is much

complex and additional variables are therefore needed to describe the kinetics of austenite formation. Factors such as particle size, distribution and chemistry of individual phases, homogeneity and the presence of non-metallic inclusions should all be important.[10-13)]

Models of specific metallurgical approaches exist for isothermal austenite formation from different initial microstructures (pure and mixed microstructures).[2,5,11,14,21-27)] However, none of these is likely to be of general applicability, except perhaps at slow heating rates consistent with the achievement of equilibrium. Thus, the main aim of this work is to study the mechanisms that control the anisothermal formation of austenite in steels with initial microstructures consisting of ferrite and/or pearlite. The influence of initial microstructure and heating rate on the transformation will be analysed. From all that theoretical knowledge and the experimental study of the mechanisms that control the formation of austenite from different initial microstructures, kinetic theory has been developed to allow the estimation of austenite formation.

Moreover, since dilatometric analysis is an alternative technique very often employed to study phase transformation kinetics in steels, the relative change in length which occurs during the austenite formation has been calculated as a function of temperature. Both kinetics and/or dilatometric analysis have been used to validate the model proposed for the non-isothermal austenite formation in steels with pure and mixed initial microstructures.

2. Materials and Experimental Procedure

2.1 Metallographic characterisation of initial microstructures

Table 1 lists the chemical composition of the studied steels. FERR1-4 steels in Table 1 have a full ferrite initial microstructure (Fig. 1). Specimens of those steels were ground and polished

using standardised techniques for metallographic examination. Nital - 2pct etching solution was used to reveal the ferrite microstructure by optical microscopy. The ferrite grain size was measured on micrographs. The average ferrite grain diameter (*D*) (Table 2) was estimated by counting the number of grains intercepted by one or more straight lines long enough to yield, at least fifty intercepts in total. The effect of a moderately non-equiaxial structure was eliminated by counting the intersections of lines in four or more orientations covering all the observation fields with an approximately equal weight.[28)]

The following heat treatments were carried out to yield in PEARL steel (Table 1) fully pearlitic microstructures with different scale parameters. Specimens were austenitised for 5 min at 1273 K, isothermally transformed at one of two different temperatures and subsequently cooled rapidly to room temperature. Table 3 lists the temperatures and holding times used for the isothermal formation of pearlite with different morphological parameters in this steel. PEARL1 specimen was ground and polished using standardised techniques and finished on 0.25 μm diamond paste for metallographic examination. An etching solution of picric acid in isopropyl alcohol with several drops of Vilella's reagent was used to reveal pearlite in this specimen on a JEOL JXA-820 scanning electron microscope (SEM) (Fig. 2.a). Pearlite in PEARL2 specimen was characterised by transmission electron microscopy (TEM). For this, 3 mm diameter cylindrical samples were sliced into 100 μm thick discs and subsequently ground down to foils of 50 μm thickness on wet 800 grit silicon carbide paper. These foils were finally electropolished at room temperature until perforation occurred, using a twin-jet electropolisher set (E. A. Fischione Inst. Mfg – Model 110) at a voltage of 100 V. The electrolyte consisted of 5 % perchloric acid, 15 % glycerol and 80 % methanol. The foils were examined in a JEOL JEM-200 CX transmission electron microscope at an operating voltage of 200 kV. (Fig. 2.b).

MIXT steel (Table 1) is a low carbon-low manganese steel with a ferrite plus pearlite initial microstructure. Semi rolled slabs 36 mm thick were soaked at 1523 K for 15 min., hot rolled to 6 mm in several passes, and finally air cooled to room temperature. The as-rolled microstructure of this steel formed by 89 % ferrite and 11 % pearlite is shown in Fig. 3.a. Specimens of this steel were polished in the usual way and finished on 0.5 μm diamond paste for metallographic examination. Two types of etching solution were used: Nital-2pct to reveal the ferrite-pearlite microstructure by light optical microscopy and solution of picric acid in isopropyl alcohol with several drops of Vilella's reagent to disclose the pearlite morphology on a JEOL JXA 840 scanning electron microscope. Figure 3.b shows a scanning micrograph of the morphology of pearlite considered in this study.

Two parameters, the mean true interlamellar spacing, σ_o, and the area per unit volume of the pearlite colonies interface, S_v^{PP}, characterise the morphology of pearlite.[14] The values of σ_o in all the cases (PEARL1-2 and MIXT specimens) were derived from electron micrographs according to Underwood's intersection procedure.[29,30]

The values of S_v^{PP} were measured on scanning micrographs by counting the number of intersections of the pearlite colony boundaries with a circular test grid as reported by Roosz et al.[14]. Approximating the pearlite colony by a truncated octahedron, the edge length of the pearlite colonies, a^P, is calculated from the area per unit volume S_v^{PP} with the following expression:[31]

$$S_v^{PP} = \frac{6\left(1+2\sqrt{3}\right)\ (a^P)^2}{8\sqrt{2}(a^P)^3} = \frac{3\left(1+2\sqrt{3}\right)}{4\sqrt{2}a^P} \qquad (1)$$

Data for σ_o, S_v^{PP} and a^P for PEARL and MIXT steels are listed in Table 4.

2.2 Dilatometric and metallographic analysis of austenite formation

The experimental validation of the austenite formation kinetics and dilatometric models developed in this work was carried out using an Adamel Lhomargy DT1000 high-resolution dilatometer.

To analyse the progress of pearlite-to-austenite transformation in PEARL steel interrupted heating experiments were carried out by quenching. Dilatometric specimens with two different scales of lamellar pearlite (PEARL1 and 2) were heated at two different constant rates (0.5 and 5 Ks^{-1}). Each test was repeated three times. Heating dilatometric curves were analysed to determine the start temperature (Ac_1) and the end temperature (Ac_3) of pearlite-to-austenite transformation and then several quench-out temperatures were selected in order to investigate the progress of the transformation. Figure 4 shows the seven selected quench-out temperatures on a dilatometric curve. They were defined as follows: $T_a=Ac_1$-5 K, $T_b=Ac_1$, T_c, T_d, and T_e, are the temperatures at the maximum, inflexion point and minimum, respectively, of the heating dilatometric curve, $T_f=Ac_3$ and $T_g=Ac_3$+10 K. All these temperatures, at which heating was interrupted by quenching for each morphology of pearlite and each heating rate, are listed in Table 5. The temperature reading presented in Table 5 corresponds to the average values of three individual tests. Austenite, which is formed inside pearlite, transforms to martensite during quenching. Thus, the progress of pearlite-to-austenite transformation is determined throughout the evolution of the volume fraction of martensite. Specimens from interrupted heating experiments were polished in the usual way for metallographic examination. Le Pera's reagent[32] was used to reveal martensite formed during quenching. The quantitative measurement of martensite volume fraction was carried out by point-counting method.[28]

Finally, to validate the dilatometric model and also, indirectly, the kinetics model for the austenite formation in FERR1-4 and MIXT steels, dilatometric specimens were heated in a vacuum of 1 Pa at a constant rate of 0.05 Ks^{-1}. Each test was repeated four times.

3. Results and Discussion

3.1 Modelling of kinetics of non-isothermal austenite formation in a steel with a ferrite initial microstructure

In the formation of austenite from ferrite, the austenite growth is controlled by processes at the interface and the growth rate G is given by:[25)]

$$G = \frac{\delta \nu}{kT} \exp\left(-\frac{\Delta G_{act}}{kT}\right) \Delta g^{\alpha \to \gamma} = \frac{\delta \nu}{kT} \exp\left(\frac{\Delta S}{k}\right) \exp\left(-\frac{\Delta H}{kT}\right) \Delta g^{\alpha \to \gamma} \{T\} \qquad (2)$$

where δ is the boundary thickness, ν is the number of attempts to jump the boundary activation barrier per unit time, k is the Boltzman constant, T is the absolute temperature, ΔG_{act} is the free energy for the activated transfer atoms across the ferrite/austenite interface, ΔS is the entropy of activation per atom, ΔH is the enthalpy of activation per atom, and $\Delta g^{\alpha \to \gamma}$ is the Gibbs free energy difference per atom between the α and γ phases. The values of ΔH and ν are uncertain but are generally assumed to be equal to the enthalpy of activation for grain boundary diffusion[33)] and to kT/h (being h Planck constant), respectively. The value of ΔS is also uncertain and may be negative or positive. If we consider that the maximum ferrite/austenite interface velocity for a 200 μm ferrite grain diameter is 0.016 m/s at 1223

K,[22] $\Delta g^{\alpha\to\gamma} = 41.87\times10^{-24}$ J per atom, δ = 5 Å, and ΔH=276.33×10^{-21} J per atom, then $\nu\exp\left(\frac{\Delta S}{k}\right)$ is equal to 1.65×10^{17} s^{-1}. Figure 5 shows the Gibbs free energy change for the ferrite-to-austenite transformation $\Delta g^{\alpha\to\gamma}$ for all the studied steels. This energy has been obtained according to the thermodynamic calculations proposed by Aaronson *et al.*[34,35] and Kaufman *et al.*.[36] In order to account for the effects of alloying elements into calculation, Zener factorisation of the free energy into magnetic and non-magnetic components has been performed.[37]

Assuming that site saturation occurs and the reaction is controlled by growth, the kinetics law obtained for the three different activated growth sites can be expressed as follows:[23,24]

$$V_\gamma = 1-\exp\left[-\left(K_s t + K_e t^2 + K_c t^3\right)\right] \tag{3}$$

where V_γ represents the formed austenite volume fraction, t is the time and K_s, K_e and K_c are given by,

$$K_s = 2G\frac{S}{V} \qquad K_e = \pi G^2\frac{L}{V} \qquad K_c = \frac{4}{3}\pi G^3\frac{C}{V} \tag{4}$$

where the growth rate of austenite (G) is given by equation (2) and $\frac{S}{V}$, $\frac{L}{V}$ and $\frac{C}{V}$ respectively are the boundary area, the edge length, and the grain corner number, all per unit volume. Assuming ferrite grains to be tetrakaidecahedra,[23] $\frac{S}{V}$, $\frac{L}{V}$ and $\frac{C}{V}$ can be expressed in terms of the average ferrite grain diameter D by: $\frac{S}{V}=\frac{3.35}{D}$; $\frac{L}{V}=\frac{8.5}{D^2}$; and $\frac{C}{V}=\frac{12}{D^3}$.

The difficulties in treating non-isothermal reactions are mainly due to the complex variations of growth rate with temperature, described in equation (2). We can only deal with the problem when the rate of transformation depends exclusively on the state of the assembly and not on the thermal path by which the state is reached.[25] Reactions of this type are called isokinetic. Avrami defined an isokinetic reaction by the condition that the nucleation and growth rates are proportional to each other (i.e. they have the same temperature variation). This leads to the concept of additivity and Scheil's rule.[38] Since Avrami's condition for an isokinetic reaction is not satisfied in the present case, a general equation to describe the non-isothermal overall ferrite-to-austenite transformation in ferritic steels was derived integrating the equation (3) over the whole temperature range where the transformation takes place.[17] In this sense, we have taken logarithms in equation (3), which then was differentiated,

$$d\left(\ln\frac{1}{1-V_\gamma}\right)=\frac{dV_\gamma}{1-V_\gamma}=\left(K_s+2K_e t+3K_c t^2\right)dt \tag{5}$$

If we consider a constant rate, $\dot{T}$, for the heating condition, time can be expressed as follows:

$$dt=\frac{dT}{\dot{T}} \qquad t=\frac{\Delta T}{\dot{T}} \tag{6}$$

substituting into equation (5) and integrating in $\lfloor 0, V_\gamma \rfloor$ and $[T_s, T]$ intervals on the left and on the right sides, respectively, it can be concluded that:

$$\int_0^{V_\gamma} \frac{dV_\gamma}{1-V_\gamma} = \int_{T_s}^{T} \left[K_s + 2K_e \frac{\Delta T}{\dot{T}} + 3K_c \frac{(\Delta T)^2}{\left(\dot{T}\right)^2} \right] \frac{dT}{\dot{T}} \tag{7}$$

where T_s is the start temperature of the transformation or temperature at which $\Delta g^{\alpha \to \gamma} = 0$ (root of the function represented in Fig. 5). Therefore, the volume fraction of austenite (V_γ) present in the microstructure as a function of temperature can be calculated as follows,

$$V_\gamma = 1 - \exp\left\{ - \int_{T_s}^{T} \left[\frac{6.7}{\dot{T}\, D} G + \frac{53.4}{\left(\dot{T}\, D\right)^2} G^2 \left(T - T_s\right) + \frac{150.8}{\left(\dot{T}\, D\right)^3} G^3 \left(T - T_s\right)^2 \right] dT \right\} \tag{8}$$

3.2 Modelling of kinetics of non-isothermal austenite formation in a steel with a pearlite initial microstructure

Nucleation and growth processes under isothermal condition can be described in general using the Avrami's equation:[39)]

$$V_\gamma = 1 - exp\left(-\frac{\pi}{3} \dot{N} G^3 t^4 \right) \tag{9}$$

where V_γ represents the formed austenite volume fraction, $\dot{N}$ is the nucleation rate, G is the growth rate and t is the time. According to Christian[25)], with a spherical configuration, an

exponent of 4 in time (t) in Avrami's equation means that the nucleation rate ($\dot{N}$) and the growth rate (G) are constant in time.

Roosz et al.[14] proposed a temperature and structure dependence of $\dot{N}$ and G as a function of the reciprocal value of overheating ($\Delta T = T\text{-}Ac_1$) as follows:

$$\dot{N} = f_N \exp\left(\frac{-Q_N}{k\Delta T}\right) \tag{10}$$

$$G = f_G \exp\left(\frac{-Q_G}{k\Delta T}\right) \tag{11}$$

where Q_N and Q_G are the activation energies of nucleation and growth, respectively, k is Boltzmann's constant, and f_N and f_G are the functions representing the influence of the structure and the heating rate on the nucleation and growth rates, respectively.

Several authors[2,14,22] reported that the nucleation of austenite inside pearlite takes place preferentially at the points of intersection of cementite with the edges of the pearlite colony. Approximating the pearlite colony as a truncated octahedron, the number of nucleation sites per unit volume is calculated as $N_C \approx \frac{1}{(a^P)^2 \sigma_\circ}$ where a^P is the edge length of the pearlite colony and σ_o is the interlamellar spacing.[31]

Bearing in mind that the rate of nucleation increases as the pearlite interlamellar spacing decreases and the edge length of the pearlite colony increases[1], and considering that the heating rate ($\dot{T}$) might influence on the nucleation rate, the function f_N in equation (10) is assumed to have the following general form:

$$f_N = K_N \frac{\left(a^P\right)^n}{\sigma_o^m}\left(\dot{T}\right)^p (N_C)^{r\dot{T}} \tag{12}$$

where K_N, n, m, p and r are empirical parameters. These parameters were adjusted in order to obtain good fit between theory and the experimental austenite volume fraction curves. In this sense, the measured values of austenite volume fraction as a function of temperature can be best described with n=6, m=1, p=$\frac{1}{2}$ and r=$\frac{1}{3}$.

Austenite nuclei in pearlite grow when carbon atoms are transported by diffusion to the ferrite/austenite boundary from the austenite/cementite boundary through the austenite and from the ferrite/cementite boundary through the ferrite, resulting in a transformation of the ferrite lattice to an austenite lattice.[5)] As in the case of the reverse transformation (austenite-to-pearlite transformation), the growth rate of austenite is believed to be controlled by either volume diffusion of carbon or by boundary diffusion of substitutional alloying elements.[37,40,41)] If the growth rate of austenite is controlled by the bulk diffusion of atoms in austenite ahead of the interface, the diffusion of carbon may play a more important role than that of substitutional alloying elements. Diffusivity of the substitutional alloying elements in austenite is far smaller than that of carbon. As a result, the substitutional alloying elements may not diffuse a long distance during the reaction. However, as described by Porter,[42)] when temperature decreases, boundary diffusion of substitutional alloying elements is the dominant mechanism in the diffusion process. In that case, the partitioning of the substitutional alloying elements is substantial during the growth of austenite and boundary diffusion of the alloying elements may control the growth rate of pearlite.

The function f_G in equation (11) representing the structure dependence on the growth rate can be expressed as follows:

$$f_G = K_G \frac{1}{\sigma_\circ^i} \tag{13}$$

where K_G is a empirical constant, i=1 if the growth rate of austenite is controlled by volume diffusion of carbon and i=2 if the growth rate of austenite is controlled by boundary diffusion of substitutional alloying elements.[14)]

As in ferrite-to-austenite transformation, a general equation to describe the non-isothermal overall pearlite-to-austenite transformation in pearlitic steel was derived integrating the Avrami's equation over the whole temperature range where the transformation takes place.[17)] In this sense, we have taken logarithms and differentiated in equation (9). Expressing time as $t = \frac{\Delta T}{\dot{T}}$ leads to:

$$\frac{dV_\gamma}{1-V_\gamma} = \frac{4\pi}{3} \dot{N} G^3 \frac{\Delta T^3}{\left(\dot{T}\right)^4} dT \tag{14}$$

Integrating in $\lfloor 0, V_\gamma \rfloor$ and $[Ac_1, T]$ intervals on the left and on the right sides of equation (14), respectively, it can be concluded that:

$$V_\gamma = 1 - exp\left(- \int_{Ac_1}^{T} \frac{4\pi}{3\left(\dot{T}\right)^4} \dot{N} G^3 \Delta T^3 dT \right) \tag{15}$$

It has been assumed that at a heating rate higher than 0.5 Ks^{-1} the growth rate of austenite would be mainly controlled by the volume diffusion of carbon in austenite, due to the fact that

the transformation would take place mostly at higher temperatures. Consequently, a *i* value of 1 is considered in equation (13) for that case. On the contrary, at heating rates lower than or equal to 0.5 Ks^{-1} the growth rate of austenite has been assumed to be controlled by boundary diffusion of substitutional alloying elements and a *i* value of 2 is considered in equation (13) for that case. The eutectoid temperature Ac_1 of the steel was obtained using Andrews' formula.[43)]

3.3 Modelling of kinetics of non-isothermal austenite formation in a steel with a ferrite plus pearlite initial microstructure

In the austenitisation of microstructures composed of ferrite and pearlite, two different transformations are involved: pearlite dissolution and ferrite-to-austenite transformation. Both transformations take place by nucleation and growth processes.

Modelling of kinetics of dissolution of pearlite

The nucleation and growth processes that control the dissolution of pearlite in a steel with a ferrite plus pearlite microstructure are the same than those described above for a steel with a full pearlite initial microstructure. Therefore, the austenite volume fraction obtained from pearlite dissolution, V_γ^P, during continuous heating of a ferrite plus pearlite initial microstructure is expressed as follows:

$$V_\gamma^P = V_{P_o}\left\{1 - exp\left(- \int_{Ac_1}^{T} \frac{4\pi}{3\left(\dot{T}\right)^4} \dot{N}\, G^3 \Delta T^3 dT \right)\right\} \qquad (16)$$

where V_{P_o} is the volume fraction of pearlite present in the initial microstructure. V_{P_o} = 0.11 in MIXT steel.

Modelling of kinetics of ferrite-to-austenite transformation after dissolution of pearlite

Datta et al.[26] carried out a quantitative microstructural analysis of the austenitisation kinetics of pearlite and ferrite aggregates at different intercritical annealing temperatures in a low-carbon steel containing 0.15 mass % C. At all the tested temperatures, pearlite-to-austenite transformation was complete in less than one second and the kinetics of the ferrite-to-austenite transformation at higher temperatures (T≥1143 K) were found to be different from those tested at lower temperatures (T<1143 K). In this sense, the time (t) dependence of the volume fraction of austenite V_γ at different temperatures was described by the following linear relationships:

$$\frac{V_\gamma}{1-V_\gamma} = \frac{V_\gamma^\alpha + V_{P_o}}{V_{\alpha_o} - V_\gamma^\alpha} = A + Bt \qquad \text{for } T < 1143 \text{ K} \tag{17}$$

$$\frac{V_\gamma}{1-V_\gamma} = \frac{V_\gamma^\alpha + V_{P_o}}{V_{\alpha_o} - V_\gamma^\alpha} = A' + B't^2 \qquad \text{for } T \geq 1143 \text{ K} \tag{18}$$

where V_γ^α is the austenite volume fraction formed from ferrite after complete pearlite-to-austenite transformation and, V_{P_o} and V_{α_o} are the volume fractions of pearlite and ferrite, respectively, present in the initial microstructure. The parameters *A*, *A'* and *B'* are insensitive

to temperature ($A \approx 0.20$, $A' = 0.25$ and $B' = 1.2 \times 10^{-3}\ s^{-2}$),[26] whereas B changes significantly with temperature. The temperature dependence of the kinetic parameter B has been calculated from Datta et al.[26] experimental results, being $B = 6 \times 10^{-12}(T - T_C)^{4.6}$ where T_C is the starting temperature of ferrite-to-austenite transformation and T-T_C the overheating for this transformation.

With the aim of adapting equations (17) and (18) to non-isothermal conditions, we have differentiated both equations, expressed time as $t = \dfrac{T - T_C}{\dot{T}}$, where $\dot{T}$ is the heating rate, and integrated in $\left[0, V_\gamma^\alpha\right]$ and $\left[T_C, T\right]$ intervals on the left and on the right sides of equation (17), respectively, and in $\left[V_D^\alpha, V_\gamma^\alpha\right]$ and $\left[T_D, T\right]$ intervals on the left and on the right sides of equation (18), respectively. T_C is the previously cited temperature and T_D the temperature at which the kinetics of ferrite-to-austenite transformation changes under non-isothermal conditions. It should be noticed that these critical temperatures do not have to correspond with those from Datta et al. study since their work was carried out under isothermal conditions. Therefore, it can be concluded that:

$$\int_0^{V_\gamma^\alpha} \frac{dV_\gamma^\alpha}{\left(V_{\alpha_o} - V_\gamma^\alpha\right)^2} = \int_{T_C}^{T} \frac{B}{\dot{T}} dT \qquad \text{for } T_C < T < T_D \tag{19}$$

$$\int_{V_D^\alpha}^{V_\gamma^\alpha} \frac{dV_\gamma^\alpha}{\left(V_{\alpha_o} - V_\gamma^\alpha\right)^2} = \int_{T_D}^{T} \frac{2B'}{\left(\dot{T}\right)^2} dT \qquad \text{for } T \geq T_D \tag{20}$$

where V_D^α is the austenite volume fraction formed from ferrite at T_D temperature.

Thus, the volume fraction of austenite formed from ferrite during continuous heating at a given temperature is expressed as follows:

$$V_\gamma^\alpha = V_{\alpha_o}\left[1-\frac{5.6\dot{T}}{6\times10^{-12}V_{\alpha_o}\left(T-T_C\right)^{5.6}+5.6\dot{T}}\right] \qquad \text{for } T_C < T < T_D \qquad (21)$$

$$V_\gamma^\alpha = V_{\alpha_o}-\frac{\left(V_{\alpha_o}-V_D^\alpha\right)\left(\dot{T}\right)^2}{\left(\dot{T}\right)^2+1.2\times10^{-3}\left(V_{\alpha_o}-V_D^\alpha\right)\left[\left(T-T_C\right)^2-\left(T_D-T_C\right)^2\right]} \qquad \text{for } T \geq T_D \qquad (22)$$

T_C and T_D temperatures were determined experimentally for MIXT steel by means of dilatometric analysis. Figure 6 shows the experimental dilatometric curve of the MIXT steel for a heating rate of 0.05 Ks^{-1}. T_C and T_D temperatures are displayed on the dilatation curve in accordance with their definition above. Ac_1 and Ac_3 critical temperatures represent the starting and finishing temperatures of the austenitisation process. The possibility to be able to discriminate the pearlite dissolution process and the ferrite-to-austenite transformation on the dilatometric curve permitted the experimental determination of T_C in this steel. This temperature has been also verified by metallography (T_C=1023 K).[21] Moreover, as Datta et al.[26] found under isothermal conditions, a change in ferrite-to-austenite growth kinetics has been also detected in this work by the above mentioned technique enabling T_D experimental determination. The small contraction after the relative change in length reached to a minimum corresponds to the formation of austenite from some grains of ferrite that remains untransformed in the microstructure. This would explain the change in the linear thermal expansion as those residual ferrite grains transform almost instantaneously at T_D temperature due to the change in ferrite-to-austenite transformation kinetics.

Figure 7 represents the calculated volume fraction of the different microconstituents as a function of temperature. From this diagram it can be seen that the eutectoid transformation (pearlite curve) proceeds within a narrow temperature range (between Ac_1 and T_C temperatures). This transformation needs about 15 K to reach completion in MIXT steel for a heating rate of 0.05 Ks^{-1}. The austenite curve clearly reproduces the two different growth kinetics that occur during ferrite-to-austenite transformation. At temperatures lower than T_D, the transformation reproduces a usual kinetic behaviour, whereas at temperatures higher than T_D, the kinetics suddenly increases promoting the completion of austenitisation process only a few degrees after.

3.4 Modelling of dilatometric behaviour of non-isothermal austenite formation

Assuming that the sample expands isotropically, the change of the sample length ΔL referred to the initial length L_o at room temperature is related to volume change ΔV and initial volume V_o at room temperature for small changes as follows:

$$\frac{\Delta L}{L_o} = \frac{V - V_o}{3V_o} \tag{23}$$

Therefore, $\frac{\Delta L}{L_o}$ can be calculated from the volumes of the unit cells and the volume fractions of the different phases present in the microstructure at every temperature during continuous heating:

$$\frac{\Delta L}{L_o} = \frac{1}{3}\left[\frac{\left(2V_\alpha\ a_\alpha^3 + \frac{1}{3}V_\theta\ a_\theta\ b_\theta\ c_\theta + V_\gamma\ a_\gamma^3\right) - \left(2V_{\alpha_o} a_{\alpha_o}^3 + \frac{1}{3}V_{\theta_o} a_{\theta_o} b_{\theta_o} c_{\theta_o}\right)}{\left(2V_{\alpha_o} a_{\alpha_o}^3 + \frac{1}{3}V_{\theta_o} a_{\theta_o} b_{\theta_o} c_{\theta_o}\right)}\right] \quad (24)$$

with $V_{\theta_o} = 0.12V_{P_o}$ and $V_{\alpha_o} = 1 - 0.12V_{P_o}$ being $V_{P_o,\alpha_o,\theta_o}$ the initial volume fractions of pearlite, ferrite and cementite, respectively, present in the microstructure at room temperature. Likewise, $V_{\alpha,\theta,\gamma}$ are the volume fractions of ferrite, cementite and austenite, respectively, at any transformation temperature. The austenite volume fraction was calculated at every temperature using the kinetics theories described above. The factors 2 and 1/3 in equation (24) are due to the fact that, the unit cell of ferrite and cementite contain 2 and 12 iron atoms, respectively, whereas that of austenite has 4 atoms. Moreover, a_{α_o} is the lattice parameter of ferrite at room temperature, taken to be that of pure iron ($a_{\alpha_o} = 2.866$ Å); a_{θ_o}, b_{θ_o}, c_{θ_o} are the lattice parameters of cementite at room temperature,[44] given by 4.5246, 5.0885 and 6.7423 Å, respectively; and a_{γ_o} is the lattice parameter of austenite at room temperature as a function of the chemical composition of the austenite:[45,46]

$$a_{\gamma_o} = 3.573 + 0.033C + 0.00095Mn - 0.0002Ni + 0.0006Cr + 0.0031Mo + 0.0018V \quad (25)$$

where the chemical composition is measured in mass % and a_{γ_o} is in Å.

Likewise, a_α, a_θ, b_θ, c_θ, and a_γ are the lattice parameters of ferrite (α), cementite (θ) and austenite (γ) at any transformation temperature. They are calculated as follows:

$$a_\alpha = a_{\alpha_o}\left[1 + \beta_\alpha\ (T - 300)\right] \quad (26a)$$

$$a_\gamma = a_{\gamma_o}\left[1+\beta_\gamma\left(T-300\right)\right] \quad (26b)$$

$$a_\theta = a_{\theta_o}\left[1+\beta_\theta\left(T-300\right)\right] \quad (26c)$$

$$b_\theta = b_{\theta_o}\left[1+\beta_\theta\left(T-300\right)\right] \quad (26d)$$

$$c_\theta = c_{\theta_o}\left[1+\beta_\theta\left(T-300\right)\right] \quad (26e)$$

where $\beta_{\alpha,\theta,\gamma}$ are the linear thermal expansion coefficients of ferrite, cementite and austenite, respectively, in K^{-1}. The values of the linear thermal expansion of ferrite and austenite[47] considered in these calculations were $\beta_\alpha = 1.244\times10^{-5}$ K^{-1} and $\beta_\gamma = 2.065\times10^{-5}$ K^{-1}. Moreover, the thermal expansion coefficient of cementite increases with temperature.[44] Using data published by Stuart and Ridley,[44] the expression of the linear expansion coefficient as a function of temperature is:

$$\beta_\theta = 6.0\times10^{-6} + 3.0\times10^{-9}\left(T-273\right) + 1.0\times10^{-11}\left(T-273\right)^2 \quad (27)$$

where T is the temperature in K.

3.5 Experimental validation of kinetics and dilatometric calculations

Experimental validation of kinetics of non-isothermal austenite formation and dilatometric calculations in steels with a ferrite initial microstructure

The dilatation curves calculated using equation (24) for a heating rate of 0.05 Ks^{-1} in FERR1-4 steels are shown in Fig. 8 in comparison with their corresponding experimental results. In Fig. 9 the experimental and calculated results of start (T_S) and finish (T_F) temperatures of

ferrite-to-austenite transformation are compared. T_S is considered to be the temperature at which the relative change in length of the steel deviates from a linear relation with temperature during heating due to the formation of austenite; T_F has been defined as the temperature at which the sample exhibits again a linear thermal expansion relation once the ferrite-to-austenite transformation is completed. Points lying on the line of unit slope show a perfect agreement between experimental and calculated values.

The calculated curves shown in Fig. 8 suggest that the ferrite-to-austenite transformation takes place almost instantaneously (1 K). In contrast, the experiments reveal that this transformation needs between 10 and 20 K to reach completion at a heating rate of 0.05 Ks^{-1}. Additionally, Fig. 9 shows that experimental T_S and T_F temperatures are higher than those predicted for all the studied steels. Any difference between these represents some kinetic hindrance to transformation. Fig. 9 shows that the FERR1 steel transforms to austenite at temperatures which are similar to the predicted temperatures. The addition of manganese clearly leads to much larger deviations from calculated results. That may be explained by the fact that the presence of a substitutional solute retards the transformation to austenite because it is necessary for the solute to diffuse during transformation.[19)]

In general, the calculated relative change in length was consistent with the measured value at every temperature. The fact that both the modelled and the experimental dilatometric curves run parallel is irrelevant as long as the adequate thermal expansion coefficients are calculated adequately.[17)] The linear expansion coefficients of ferrite and austenite from Takahashi[47)] are in a good agreement with those measured values.

Experimental validation of the pearlite dissolution model in a steel with a pearlite initial microstructure

Figure 10 shows the experimental and calculated austenite formation kinetics plotted as a function of temperature for two different morphologies of pearlite (PEARL1 and 2) and two different constant rates (0.5 and 5 Ks^{-1}). R^2 is the square correlation factor of the experimental and calculated volume fraction of austenite formed at different temperatures. This parameter quantifies the accuracy of the model. The figure suggests that austenite transformation starts later and appears to be slower the coarser the initial pearlite microstructure and the higher the heating rate. Experimental results for the austenite volume fraction are in good agreement with the predicted values from the model proposed in this work (section 3.2). The accuracy of this model is in the two cases higher than 90% which can be considered excellent for a kinetics model bearing in mind the experimental difficulties for its validation.

Experimental validation of kinetics of non-isothermal austenite formation and dilatometric calculations in steels with a ferrite plus pearlite initial microstructure

The dilatation curve calculated using equation (24) for MIXT steel with a mixed initial microstructure consisting of ferrite and pearlite under continuous heating conditions (0.05 Ks^{-1} of heating rate) is shown in Fig. 11 in comparison with the corresponding experimental curve. For convenience of discussion, these dilatation curves can be divided in four stages according to the calculated transformation temperatures: a) from room temperature to the Ac_1 temperature at which pearlite dissolution starts; b) from Ac_1 to T_C at which pearlite dissolution finishes and ferrite-to-austenite transformation starts; c) from T_C to Ac_3 temperature at which the transformation of ferrite-to-austenite is finished; and, d) from Ac_3 to the austenitisation temperature at which non-isothermal heating finishes.

In the first stage, the experimental dilatometric curve exhibits a linear thermal expansion relation with temperature. This is because the initial microstructure of the steel remains

unchanged until Ac_1 temperature is reached. At that moment, the relative change in length of the sample no longer follows the linear relation with temperature and it contracts due to the dissolution of pearlite. With increasing temperature and already in the third stage, the relative change in length reach to a maximum, and then decreases until all ferrite is transformed into austenite. This process depends on the competition between the thermal expansion and the ferrite-to-austenite transformation. Thus, even after the relative change in length has reached to a minimum, some ferrite could remain untransformed in the microstructure. This explains the change in the linear thermal expansion as the residual ferrite transforms almost instantaneously at T_D temperature. Beyond that temperature, the sample is fully austenitised, Ac_3 temperature is reached, and the sample exhibits a linear thermal expansion relation with temperature.

In general, the calculated relative change in length was also consistent with the measured value at every temperature for this steel. The linear expansion coefficients[44,47)] of ferrite, cementite and austenite considered in calculations are in a good agreement with those measured values. Experimental kinetic transformation, critical temperatures Ac_1 and Ac_3 as well as the magnitude of the overall contraction due to austenite formation are accurately reproduced by dilatometric calculations. The only difference between both curves corresponds to the general shape of the curve between the onset and the end of the ferrite-to-austenite transformation (i.e. whether or not the specimen continued to expand for a while after the dissolution of pearlite). That discrepancy may be justified by the experimental results of a recent work.[48)] This work reported that macroscopic heterogeneous samples with respect to the rolling direction in the steel, very common in hot rolled low carbon steels, undergo an anisotropic dilatation behaviour during transformation of the steel. That possibility is not considered is this model based on isotropic expansion of the sample (see equation (23)).

4. Conclusions

1. Theoretical knowledge regarding the isothermal formation of austenite from pure and mixed initial microstructures has been used to develop a model for the non-isothermal austenite formation in a wide range of steels with an initial microstructure consisting of ferrite and/or pearlite. Since conditions to apply Scheil's rule are rarely satisfied, the Avrami's equation has been used to reproduce the kinetics of the austenite formation during continuous heating.
2. In steels with a full ferrite initial microstructure, nucleation of austenite occurs at the α/α grain boundaries. All possible nucleation sites at the grain boundaries have been taken into consideration in the modelling assuming that no nucluation barrier exists. Since ferrite/austenite boundary migrates in the absence of diffusion, the growth of austenite has been considered to be controlled by processes at the interface.
3. In the case of pearlite-to-austenite transformation, the model proposes two functions, f_N and f_G, which represent the dependence of nucleation and growth rates, respectively, on the structure and heating rate. In this sense, the influence of structure parameters, such as interlamellar spacing and edge length of pearlite colonies, and heating rate on the transformation kinetics has been experimentally studied in a eutectoid steel. It has been found that austenite transformation starts later and appears to be slower the coarser the initial pearlite microstructure and the higher the heating rate. Furthermore, both start and finish temperatures slightly increase as heating rate does, but finish temperatures of the pearlite-to-austenite transformation are more sensitive to the heating rate than start temperatures. However, the influence of heating rate on both temperatures is less significant when the finer the initial pearlite microstructure.

4. In a steel with mixed initial microstructure consisting of ferrite and pearlite, firstly, the kinetics of pearlite dissolution during continuous heating has been reproduced using the model for the kinetics of the pearlite-to-austenite transformation developed initially for steels with a full pearlite initial microstructure. Likewise, Datta et al. expressions for the kinetics of ferrite-to-austenite transformation at different intercritical annealing temperatures and a mathematical procedure consisting of reiterated differentiation and integration of kinetics functions have allowed to calculate the austenite volume fraction formed from ferrite after pearlite dissolution as a function of temperature for continuous heating conditions.
5. A model of the dilatometric behaviour of the non isothermal austenite formation has been also developed. The relative change in length which occurs during the austenitisation process has been calculated as a function of temperature.
6. Experimental validation of the kinetics model of the ferrite-to-austenite transformation has been carried out by comparison between experimental and theoretical heating dilatometric curves. Results show that experimental start and finish temperatures of the transformation are higher than those predicted for all the studied steels. Furthermore, the addition of manganese clearly leads to much larger deviations from calculated results since the presence of a substitutional solute retards the transformation to austenite.
7. Experimental results for the austenite volume fraction and critical temperatures of pearlite-to-austenite transformation for a eutectoid steel are in good agreement (accuracy higher than 90% in square correlation factor) with the predicted values from the model proposed in this work.
8. Finally, the experimental validation of the kinetics model for the ferrite+pearlite-to-austenite transformation has been carried out by comparison between experimental and theoretical heating dilatometric curves in a low carbon low manganese steel.

Transformation kinetics, critical temperatures Ac_1 and Ac_3, as well as the magnitude of the overall contraction due to austenite formation are accurately reproduced by dilatometric calculations.

Acknowledgements.-The authors acknowledge financial support from Consejería de Educación y Cultura de la Comunidad Autónoma de Madrid (CAM 07N/0065/1998).

References

1) G. A. Roberts and R. F. Mehl: *Trans. ASM*, 31 (1943), 613.
2) R. R. Judd and H. W. Paxton: *Trans. TMS-AIME*, 242 (1968), 206.
3) S. Kinoshita and R. Ueda: *Trans. Iron Steel Inst. Jpn*., 14 (1974), 411.
4) G. Molinder: *Acta Met*., 4 (1956), 565.
5) M. Hillert, K. Nilsson, and L. E. Torndahl: *Journ. of the Iron and Steel Inst*, 209 (1971), 49.
6) M. Nemoto: *Met. Trans. A*, 8A (1977), 431.
7) G. Krauss: Steels: Heat Treatment and Processing Principles, ASM International, Ohio, (1989), 274
8) A. Gustavsson, D. L. Mcdowell, A. Melander, and M. Larsson: *Inst. Metallforsk. Forsk. Rapp*., 88 (1994), 3145.
9) V. L. Gadgeel: *Tool Alloy Steels*, 28 (1994), 17.
10) C. I. García and A. J. DeArdo: *Met. Trans. A*, 12A (1981), 521.
11) G. R. Speich, V. A. Demarest and R. L. Miller: *Met. Trans. A*, 12A (1981), 1419.
12) M. M. Souza, J. R. C. Guimaraes and K. K. Chawla: *Met. Trans. A*, 13A (1982), 575.
13) Xue-Ling Cai, A. J. Garrat-Reed and W. S. Owen: *Met. Trans. A*, 16A (1985), 543.
14) A. Roosz, Z. Gacsi and E. G. Fuchs: *Acta Metall.*, 31 (1983), 509.
15) H. K. D. H. Bhadeshia and L. E. Svensson: Mathematical Modelling of Weld Phenomena, The Institute of Materials, London, (1993), 109.
16) J. R. Yang and H. K. D. H. Bhadeshia: *Materials Science and Engeneering*, A131 (1991), 99.
17) C. García de Andrés, F. G. Caballero, C. Capdevila and H. K. D. H. Bhadeshia: *Scripta Materiallia*, 39 (1998), 791.

18) F.G. Caballero, C. Capdevila and C. García de Andrés: *Scripta Materiallia*, 42 (2000), 1159.

19) L. Gavard, H. K. D. H. Bhadeshia, D. J. C. MacKay, and S. Suzuki: *Materials Science and Technology*, 12 (1996), 453.

20) C. A. L. Bailer-Jones, H. K. D. H. Bhadeshia and D. J. C. MacKay: *Materials Science and Technology*, 15 (1999), 287.

21) C. García de Andrés, F. G. Caballero and C. Capdevila: *Scripta Mater.*, 38 (1998), 1835.

22) G. R. Speich and A. Szirmae: *Trans. TMS-AIME*, 245 (1969), 1063.

23) J. W. Cahn: *Acta Metall*., 4 (1956), 449.

24) S. F. Dirnfeld, B. M. Korevaar and F. Van't Spijker: *Metall. Trans.*, 5 (1974), 1437.

25) J. W. Christian: The Theory of Transformations in Metals and Alloys, Pergamon Press, Oxford, (1965), 19.

26) D. P. Datta and A. M. Gokhale: *Metall. Trans. A.*, 12A (1981), 443.

27) E. Navara and R. Harrysson: *Scripta Metall.*, 18 (1984), 605.

28) G. F. Vander Voort: Metallography. Principles and Practice, McGraw-Hill, New York, (1984), 427.

29) E. E. Underwood: Quantitative Stereology, Addison-Wesley Publishing Co, Reading, (1970), 73.

30) S. A. Saltykov: Stereometric Metallography, Metallurgizdat, Moscow, (1958), 267.

31) R. T. De Hoff and F.H. Rhines: Quantitative Stereology, McGraw-Hill, New York, (1968), 93.

32) F. S. Le Pera: *J. of Metals*, 32 (1980), 38.

33) P. Shewmon: Diffusion in Solids, McGraw-Hill, New York, (1963), 166.

34) H. I. Aaronson, H. A. Domian and G. M. Pound: *Trans. TMS-AIME*, 236 (1966)**,** 753.

35) H. I. Aaronson, H. A. Domian and G. M. Pound: *Trans. TMS-AIME*, 236 (1966)**,** 768.

36) L. Kaufman, E. V. Clougherty and R. J. Weiss: *Acta Metall.*, 11 (1963), 323.

37) C. ZENER: *Trans. AIME*, 167 (1946), 550.

38) R. G. Kamat, E. B. Hawbolt, L. C. Brown and J. K. Brimacombe: *Metall. Trans.*, 23A (1992), 2469.

39) M. Avrami: *J. Chem. Phys.*, 8 (1940), 212.

40) M. Hillert: *Jernkont. Ann.*, 141 (1957), 757.

41) M. Hillert: The Mechanism of Phase Transformation in Crystalline Solids, Institute of Metals, London, (1969), 231.

42) D. A. Porter and K. E. Easterling: Phase Transformations in Metals and Alloy, 2nd ed., Chapman and Hall, London, (1992), 101.

43) K. W. Andrews: *JISI*, 203 (1965), 721.

44) H. Stuart and N. Ridley: *JISI*, 204 (1966), 711.

45) N. Ridley, H. Stuart, and L. Zwell: *Trans. of A.I.M.E.*, 245 (1969), 1834.

46) D. J. Dyson and B. Holmes: *JISI*, 208 (1970), 469.

47) M. Takahashi: Reaustenitization from Bainite in Steels, University of Cambridge, Cambridge, (1992), 91.

48) T. A. Kop: A dilatometric study of the austenite/ferrite interface mobility, Delft University of Technology, Enschede, (2000), 30.

Table 1. Chemical composition (mass %).

Table 2. Average ferrite grain diameter in ferritic steels

Table 3. Isothermal conditions employed for the formation of pearlitic microstructures in PEARL steel.

Table 4. Morphological characterisation of pearlite in PEARL and MIXT steels.

Table 5. Temperatures in K of heating interruption by quenching in PEARL steel.

Fig. 1. Optical micrograph of a full ferrite microstructure. FERR1 steel

Fig. 2. Electron micrographs of the two different morphologies of pearlite in PEARL steel (Table 3): (a) PEARL1 (SEM); (b) PEARL2 (TEM).

Fig. 3. Initial microstructure of MIXT steel: (a) Optical micrograph; (b) Scanning electron micrograph.

Fig. 4. Temperatures selected from heating dilatometric curves to investigate the progress of pearlite-to-austenite transformation in a eutectoid steel.

Fig. 5. Gibbs free energy change for $\alpha \rightarrow \gamma$ transformation in FERR1-4 steels

Fig. 6. Experimental dilatation curve, average of four identical dilatometric tests, of the MIXT steel for a heating rate of 0.05 Ks^{-1}.

Fig. 7. Calculated volume fraction of the different phases present in the microstructure as a function of temperature for MIXT steel.

Fig. 8. Calculated dilatation curve of FERR1-4 compared with their corresponding experimental curves obtained at a heating rate of 0.05 Ks^{-1}

Fig. 9. Comparison of experimental and calculated start (T_S) and finish (T_F) temperatures of ferrite-to-austenite transformation in FERR1-4 steels for a heating rate of 0.05 Ks^{-1}

Fig. 10. Experimental and calculated kinetics results for the formation of austenite inside pearlite under continuous heating conditions in PEARL steel.

Fig. 11. Calculated and experimental dilatation curves of MIXT steel for a heating rate of 0.05 Ks^{-1}.

Table 1 Chemical composition (mass %)

Steels	C	Mn	Si	N	Al	P	Cr	Ni
FERR1	0.002	0.05	-	0.004	-	0.003	-	-
FERR2	0.010	0.25	0.028	0.003	0.057	0.016	0.014	0.022
FERR3	0.010	0.37	0.028	0.002	0.069	0.016	0.016	0.022
FERR4	0.010	0.50	0.028	0.004	0.046	0.015	0.012	0.020
PEARL	0.76	0.91	0.24	-	-	0.013	-	-
MIXT	0.11	0.50	0.028	0.004	0.046	0.015	0.012	0.020

Table 2 Average ferrite grain diameter in ferritic steels

Steels	*D* (μm)
FERR1	158±28
FERR2	21±3
FERR3	63±11
FERR4	17±1

Table 3. Isothermal conditions employed for the formation of pearlitic microstructures in PEARL steel

Specimen	Temperature (K)	Time (min)
PEARL1	948	45
PEARL2	798	60

Table 4 Morphological characterisation of pearlite in PEARL and MIXT steels

Specimen	$\sigma_o \times 10^{-3}$ (mm)	S_v^{PP} (mm^{-1})	$a^P \times 10^{-3}$ (mm)
PEARL1	0.20±0.03	581±86	4.16±0.70
PEARL2	0.06±0.01	1432±60	1.65±0.07
MIXT	0.15±0.02	959±154	2.50±0.50

Table 5 Temperatures in K of heating interruption by quenching in PEARL steel

Morphology of Pearlite	Heating Rate (Ks^{-1})	T_a	T_b	T_c	T_d	T_e	T_f	T_g
PEARL1	0.5	1005	1010	1011	1018	1026	1031	1041
	5	1014	1019	1023	1026	1041	1050	1060
PEARL2	0.5	998	1003	1006	1011	1017	1020	1030
	5	1001	1006	1008	1011	1019	1031	1041

Fig. 1. Optical micrograph of a full ferrite microstructure. FERR1 steel

(a)

(b)

Fig. 2. Electron micrographs of the two different morphologies of pearlite in PEARL steel (Table 3): (a) PEARL1 (SEM); (b) PEARL2 (TEM)

(a)

(b)

Fig. 3. Initial microstructure of MIXT steel: (a) Optical micrograph; (b) Scanning electron micrograph

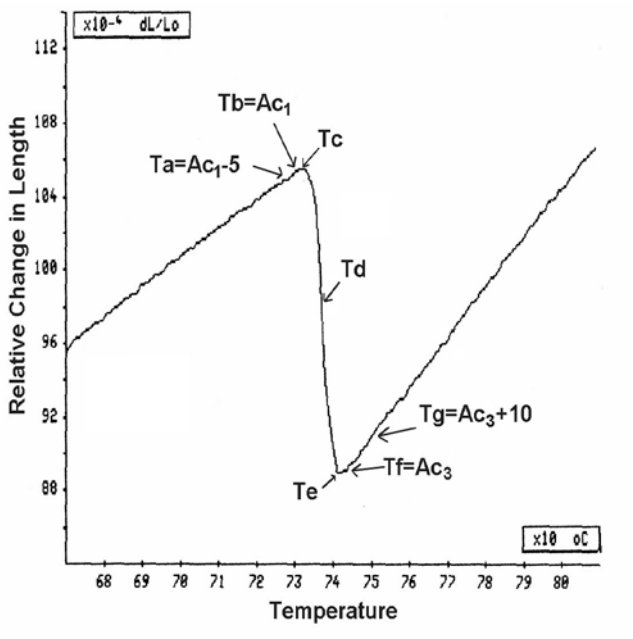

Fig. 4. Temperatures selected from heating dilatometric curves to investigate the progress of pearlite-to-austenite transformation in a eutectoid steel

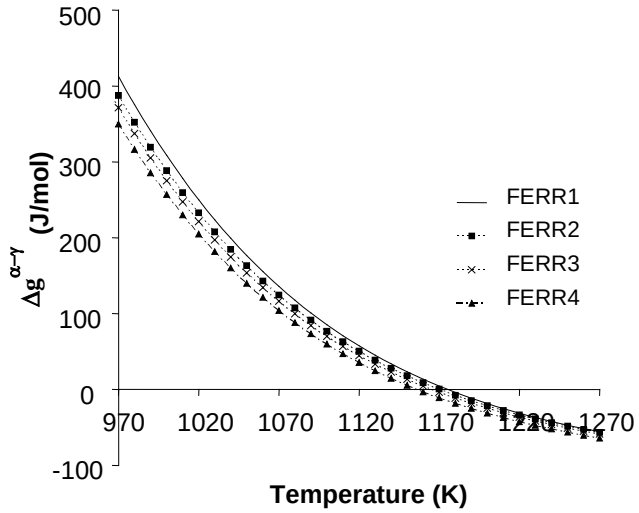

Fig. 5. Gibbs free energy change for $\alpha \rightarrow \gamma$ transformation in FERR1-4 steels

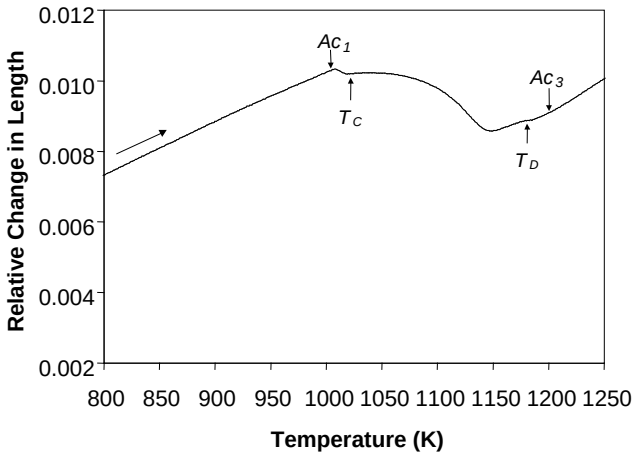

Fig. 6. Experimental dilatation curve, average of four identical dilatometric tests, of the MIXT steel for a heating rate of 0.05 Ks^{-1}

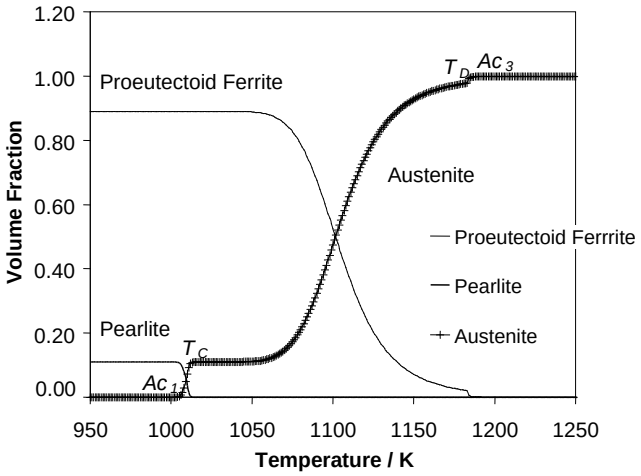

Fig. 7. Calculated volume fraction of the different phases present in the microstructure as a function of temperature for MIXT steel

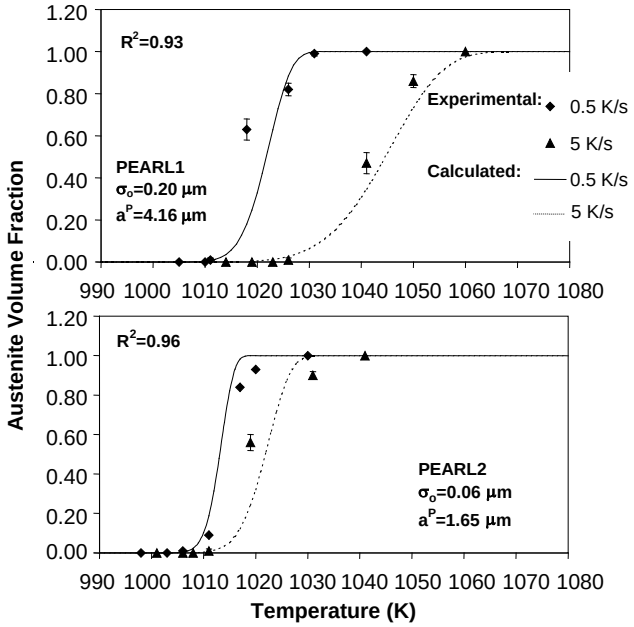

Fig. 10. Experimental and calculated kinetics results for the formation of austenite inside pearlite under continuous heating conditions in PEARL steel

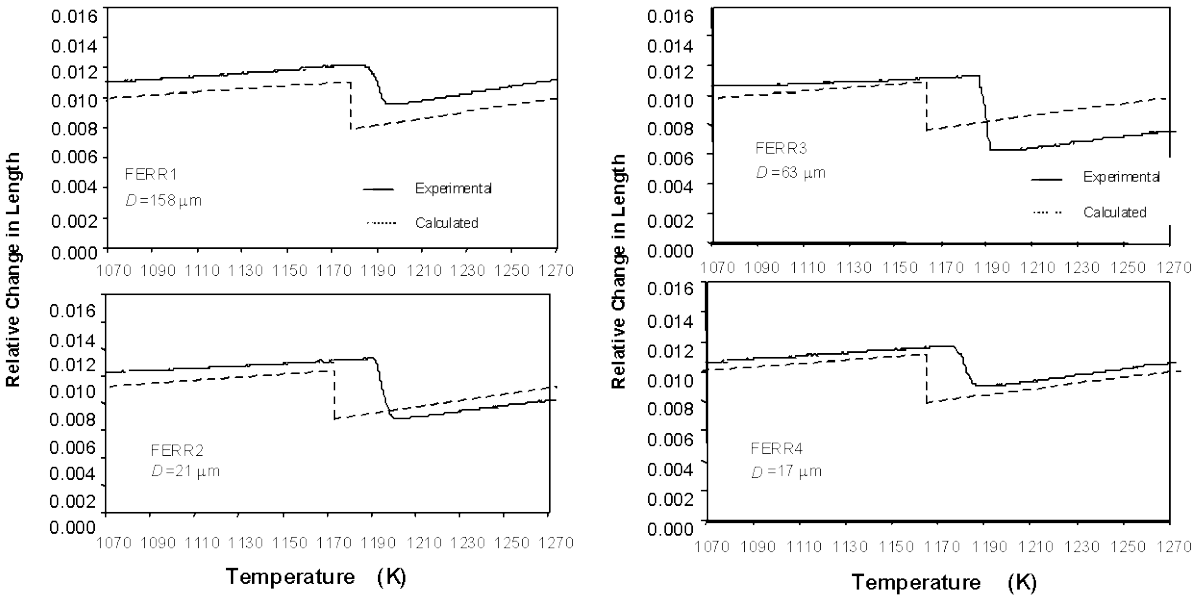

Fig. 8. Calculated dilatation curve of FERR1-4 compared with their corresponding experimental curves obtained at a heating rate of 0.05 Ks^{-1}

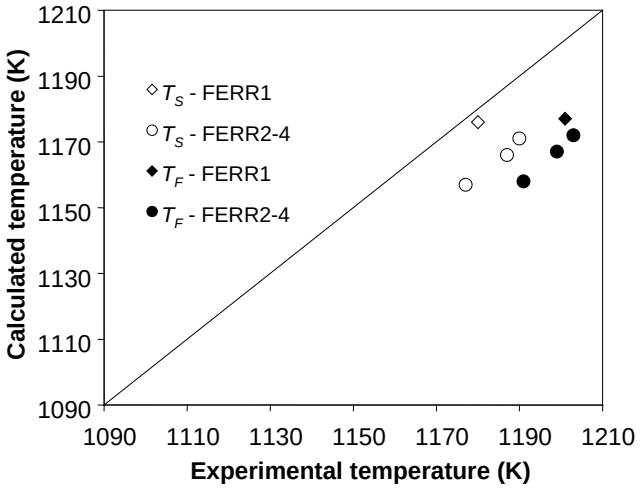

Fig. 9. Comparison of experimental and calculated start (T_S) and finish (T_F) temperatures of ferrite-to-austenite transformation in FERR1-4 steels for a heating rate of 0.05 Ks^{-1}

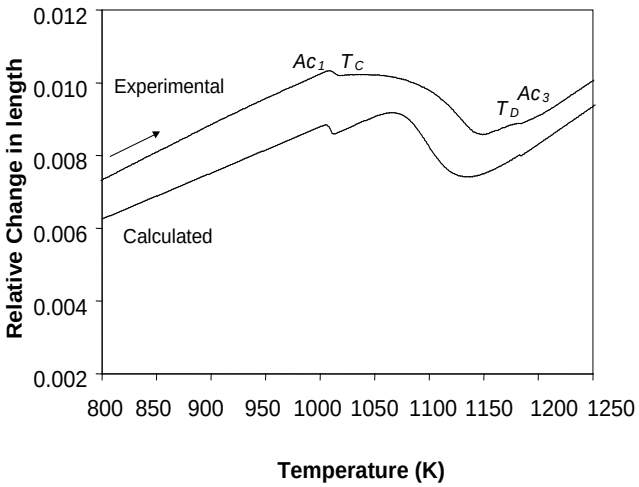

Fig. 11. Calculated and experimental dilatation curves of MIXT steel for a heating rate of 0.05 Ks^{-1}